JOURNAL OF RAMAN SPECTROSCOPY
J. Raman Spectrosc. **31**, 41–49 (2000)

Femtosecond spectrally dispersed three-pulse four-wave mixing: the role of sequence and chirp in controlling intramolecular dynamics

Vadim V. Lozovoy,† Bruna I. Grimberg, Emily J. Brown, Igor Pastirk‡ and Marcos Dantus*
Department of Chemistry and Center for Fundamental Materials Research, Michigan State University, East Lansing, Michigan 48824, USA

The roles of pulse sequence and pulse chirp were explored using femtosecond three-pulse four-wave mixing (FWM). The experiments were carried out on gas-phase I_2 and the degenerate laser pulses are resonant with the transition between the X ($^1\Sigma_{g+}$) ground and B ($^3\Pi_{0u+}$) excited electronic states. Impulsive excitation leads to the observation of vibrational coherence in the ground and the excited states. Control over the observed population and vibrational coherence is achieved by using specific pulse sequences. Using chirped pulses results in changes in vibrational coherence. When the FWM signal is spectrally dispersed, the two-dimensional data (wavelength and time delay) provide important spectroscopic information about the intramolecular dynamics of both electronic states. This information is not typically available in time or spectrally integrated measurements. A theoretical foundation for these observations based on the density matrix formalism is briefly discussed.

INTRODUCTION

Time-resolved non-linear spectroscopic techniques have been used for the study of isolated molecules since the early 1970s.[1,2] Since the mid-1980s, femtosecond lasers have been used to study short-lived species (10^{-12} s), transition states of chemical reactions and high-resolution vibrational and rotational spectra of bound systems.[3–6] The impulsive excitation achieved with short laser pulses leads to the observation of wave packet dynamics in real time. These observations have been carried out in gases, liquids and solids. In most of these time-resolved measurements, the goal has been to keep the laser chirp (a time-dependent frequency sweep over the pulse) to a minimum in order to ensure maximum temporal resolution.[3–6] More recently, several research groups have explored the use of chirped laser pulses, for example to enhance population transfer or excite high vibrational levels of molecules in the gas phase.[7] Here we deliberately used laser chirp to study its effect on femtosecond three-pulse four-wave mixing (FWM) spectroscopy. We also explored the use of different pulse sequences to control the observed vibrational coherence from the ground and the excited states.

In general, the transfer of population from one state to another following resonant excitation is described by the transition probability $|\langle e|\mu \cdot \mathbf{E}(t)|g\rangle|^2 = \langle e|\mu \cdot \mathbf{E}(t)|g\rangle\langle g|\mu \cdot \mathbf{E}(t)^*|e\rangle$, where $\mathbf{E}(t)$ is the applied electric field and μ is the transition dipole moment that couples both electronic states. Efforts to control the population transfer process between two electronic levels have followed two general schemes, the creation of a π-pulse[8] or techniques using two different electric field interactions where these electric fields are correlated in phase.[9–11] Otherwise, the competition between absorption and stimulated emission limits the extent of population transfer and prevents population inversion. Phase-matched three-pulse FWM provides a spectroscopic tool in which the electric field of each laser pulse interacts once on the system. Thus, in addition to using phase-locked laser pulses,[9] techniques using a phase-matched geometry can also lead to control of the coherent part of this process.

Here we explore the effect of pulse sequences on the observed dynamics of I_2. Specifically, the time delay between the first two laser pulses (τ_{ab}) has been systematically changed. For each time delay, data are obtained by scanning the third pulse in time (τ). In addition, we have explored the role of chirp on the observed dynamics. The information provided by time-resolved FWM is not sufficient to appreciate fully the complex ground- and excited-state intramolecular dynamics that ensue upon impulsive excitation. We spectrally dispersed the FWM signal in order to obtain two-dimensional information (time and wavelength). The resulting experimental data support the fact that pulse sequences and chirp can be used to control coherence and population transfer between the ground and excited states of I_2.

Materny and Kiefer's group has explored the molecular dynamics of I_2 using a three-pulse FWM setup with femtosecond laser beams. Their measurement used two pulses overlapped in time with the third pulse scanned in time (Δt) and resulted in the observation of ground- and excited-state dynamics.[12] When $\Delta t < 0$ (scanning pulse arrives before the overlapped ones), only excited

* Correspondence to: M. Dantus, Department of Chemistry and Center for Fundamental Materials Research, Michigan State University, East Lansing, Michigan 48824, USA.
E-mail: dantus@cem.msu.edu
† Permanent address: N. N. Semenov, Institute of Chemical Physics, RAS, Moscow, Russia.
‡ Affiliated with the Institute for Nuclear Sciences 'VINCA,' Belgrade, F. R. Yugoslavia.
Contract/grant sponsor: National Science Foundation; Contract/grant number: CHE-9812584.

CCC 0377–0486/2000/010041–09 $17.50

Received 30 July 1999
Accepted 10 August 1999

dynamics were observed. However, for $\Delta t > 0$ (overlapped pulses arrive before the scanning one), both ground and excited state dynamics were observed. Our group recently observed similar dynamics at a slightly different wavelength.[13]

The above dynamics were observed when detecting the signal at the central wavelength of the laser spectral profile (i.e. degenerate setup). Schmitt *et al*. have also examined the relationship between signal detection wavelength and the observed dynamics.[14] They found that detecting the signal at a shorter wavelength (CARS) resulted in observing only excited-state dynamics for $\Delta t < 0$ and only ground-state dynamics for $\Delta t > 0$. When they detected the signal at a longer wavelength (CSRS), no signal oscillations were observed for $\Delta t < 0$ while for $\Delta t > 0$ excited-state dynamics were observed.

Using specific pulse sequences we were able to isolate the processes leading to the observation of ground- or excited-state dynamics.[16] We also explored the role of laser chirp on the observed vibrational coherence. Our paper is organized as follows. First we briefly discuss the theoretical foundation for interpreting the three-pulse FWM signal. The subsequent section gives experimental details regarding three-pulse FWM, then experimental results are presented for different time delays and chirp values. An experimental application is also presented using pulse sequences for determining T_2 values for the ground and excited states of I_2. Finally, some theoretical generalizations regarding the role of chirp are given.

THEORY

The purpose of this section is to introduce a formalism that makes apparent the control mechanism of our experiment. The density matrix formulation[15] is a suitable theoretical approach for the study of a multi-wave mixing experiment[16,17] when the coherence effects are important.[18] The time evolution of the density matrix elements is obtained from the solution of the Liouville equation. In the weak interaction limit, each dipole interaction with successive electric fields, $E^{(n)}(t - t_n)$, will produce a change of order $\rho^{(n)}(t)$ in the density matrix.

The simulation of the experimental results is based on a four-level system, two electronic states with two vibrational levels each, labeled $|1\rangle$, $|2\rangle$, $|3\rangle$ and $|4\rangle$. When the three electric fields interact with the system, the density matrix evolves as

$$\begin{pmatrix} \rho_{11}^{0} & 0 & 0 & 0 \\ 0 & \rho_{22}^{0} & 0 & 0 \\ 0 & 0 & 0 & 0 \\ 0 & 0 & 0 & 0 \end{pmatrix} \xrightarrow{E^{(1)}(t)} \begin{pmatrix} 0 & 0 & \rho_{13}^{(1)} & \rho_{14}^{(1)} \\ 0 & 0 & \rho_{23}^{(1)} & \rho_{24}^{(1)} \\ \rho_{31}^{(1)} & \rho_{32}^{(1)} & 0 & 0 \\ \rho_{41}^{(1)} & \rho_{42}^{(1)} & 0 & 0 \end{pmatrix}$$

$$\xrightarrow{E^{(2)}(t-\tau_{ab})} \begin{pmatrix} \rho_{11}^{(2)} & \rho_{12}^{(2)} & 0 & 0 \\ \rho_{21}^{(2)} & \rho_{22}^{(2)} & 0 & 0 \\ 0 & 0 & \rho_{33}^{(2)} & \rho_{34}^{(2)} \\ 0 & 0 & \rho_{43}^{(2)} & \rho_{44}^{(2)} \end{pmatrix}$$

$$\xrightarrow{E^{(3)}(t-(\tau_{ab}+\tau))} \begin{pmatrix} 0 & 0 & \rho_{13}^{(3)} & \rho_{14}^{(3)} \\ 0 & 0 & \rho_{23}^{(3)} & \rho_{24}^{(3)} \\ \rho_{31}^{(3)} & \rho_{32}^{(3)} & 0 & 0 \\ \rho_{41}^{(3)} & \rho_{42}^{(3)} & 0 & 0 \end{pmatrix} \tag{1}$$

Following the first pulse, we recover only the matrix elements corresponding to the electronic coherence, $\rho_{ge}^{(1)}(t)$ (upper right block) and $\rho_{eg}^{(1)}(t)$ (lower left block) where the index $g = 1$ or 2 and index $e = 3$ or 4. When the second field is applied at time τ_{ab}, a spatial transient grating is formed in the sample. The interaction of the molecules with the two electric fields produces changes in the populations of the ground and the excited states, $\rho_{gg}^{(2)}(\tau_{ab})$ (upper left) and $\rho_{ee}^{(2)}(\tau_{ab})$ (lower right), and consequently changes in the vibrational coherence, $\rho_{gg'}^{(2)}(t, \tau_{ab})$ and $\rho_{ee'}^{(2)}(t, \tau_{ab})$. Interaction with the third pulse at time $\tau_{ab} + \tau$ produces an electronic coherence $\rho_{ge}^{(3)}(t)$ resulting in a polarization, $P^{(3)}(t, \tau_{ab}, \tau)$, of the molecules that are either in the excited or ground state after the interaction with the first two pulses. This non-linear polarization is the source of a new field, $E_S(t, \tau_{ab}, \tau)$, that is emitted in a phase-matching direction producing an optical signal:

$$I_{FWM}(\tau_{ab}, \tau) \propto \int_{-\infty}^{\infty} |Tr[\hat{P}\hat{\rho}^{(3)}(t, \tau_{ab}, \tau)]|^2 \mathrm{d}t \tag{2}$$

where $\hat{P}$ is the polarization operator and Tr denotes the trace operator. Therefore, in order to simulate the signal, we need to calculate $\hat{\rho}^{(3)}(t, \tau_{ab}, \tau)$. Note, however, that the preparation of the ground- and excited-state wave packets depends on the first two pulses. This is apparent in the expression of $\hat{\rho}^{(2)}(t, \tau_{ab})$ (see below).

We derive the expression of $\hat{\rho}^{(2)}(t, \tau_{ab})$ when the carrier frequency of the applied electric fields ω is resonant with the electronic transition between the ground and the excited state. We assume short pulses that do not overlap in time, $E_a(t)$ and $E_b(t)$, with spectral chirp ϕ_a'' and ϕ_b'' and wavevectors $\mathbf{k}_a$ and $\mathbf{k}_b$, respectively. When initially the molecules are equally distributed into the ground-state vibrational levels ($\rho_{11}^0 = \rho_{22}^0$), the expressions of the population matrix elements after two pulses are

$$\begin{aligned} \rho_{gg}^{(2)} = &-(A/2)^2 \cos\left(\tfrac{1}{2}\omega_e\tau_{ab} \mp \tfrac{1}{2}\omega_g\omega_e\Delta\phi''\right) \\ &\times \cos\left[\left(\tfrac{1}{2}\omega_g \pm \omega\right)\tau_{ab} - (\mathbf{k}_a - \mathbf{k}_b)\cdot\mathbf{x}\right. \\ &\left. + \tfrac{1}{4}\left(\omega_g^2 + \omega_e^2\right)\Delta\phi''\right] \end{aligned} \tag{3a}$$

and

$$\begin{aligned} \rho_{ee}^{(2)} = &-(A/2)^2 \cos\left(\tfrac{1}{2}\omega_g\tau_{ab} \mp \tfrac{1}{2}\omega_g\omega_e\Delta\phi''\right) \\ &\times \cos\left[\left(\omega \mp \tfrac{1}{2}\omega_e\right)\tau_{ab} + (\mathbf{k}_a - \mathbf{k}_b)\cdot\mathbf{x}\right. \\ &\left. - \tfrac{1}{4}\left(\omega_g^2 + \omega_e^2\right)\Delta\phi''\right] \end{aligned} \tag{3b}$$

where A is the area under pulse,[19,20] $\Delta\phi'' = \phi_a'' - \phi_b''$, $\mathbf{x}$ the spatial coordinate and ω_g and ω_e are the vibrational frequencies of the ground and excited state, respectively. The upper and lower sets of signs in Eqn (3a) correspond to $g = 1$ and $g = 2$, respectively, and similarly for $e = 3$ and $e = 4$ in Eqn (3b). The vibrational coherence matrix elements are

$$\begin{aligned} \rho_{gg'}^{(2)}(t) = &(A/2)^2 \mathrm{e}^{-i\omega_g(t-\tau_{ab}/2)} \\ &\times \left\{ \begin{array}{l} \cos\left(\tfrac{1}{2}\omega_e\tau_{ab}\right)\cos\left(\tfrac{1}{2}\omega_g\omega_e\Phi''\right)\cos\left[\omega\tau_{ab}\right. \\ \left. - (\mathbf{k}_a - \mathbf{k}_b)\cdot\mathbf{x} - \tfrac{1}{4}(\omega_g^2 + \omega_e^2)\Delta\phi''\right] \\ + \sin\left(\tfrac{1}{2}\omega_e\tau_{ab}\right)\sin\left(\tfrac{1}{2}\omega_g\omega_e\Phi''\right)\sin[\omega\tau_{ab} \\ - (\mathbf{k}_a - \mathbf{k}_b)\cdot\mathbf{x} - \tfrac{1}{4}(\omega_g^2 + \omega_e^2)\Delta\phi''] \end{array} \right\} \end{aligned} \tag{3c}$$

and

$$\rho^{(2)}_{ee'}(t) = (A/2)^2 \mathrm{e}^{-i\omega_e(t-\tau_{ab}/2)} \times \left\{ \begin{array}{l} \cos\left(\frac{1}{2}\omega_g\tau_{ab}\right)\cos\left(\frac{1}{2}\omega_g\omega_e\Phi''\right)\cos\left[\omega\tau_{ab} \right. \\ \left. -(\mathbf{k}_a-\mathbf{k}_b)\cdot\mathbf{x}-\frac{1}{4}(\omega_g^2+\omega_e^2)\Delta\phi''\right] \\ +\sin\left(\frac{1}{2}\omega_g\tau_{ab}\right)\sin\left(\frac{1}{2}\omega_g\omega_e\Phi''\right)\sin[\omega\tau_{ab} \\ -(\mathbf{k}_a-\mathbf{k}_b)\cdot\mathbf{x}-\frac{1}{4}(\omega_g^2+\omega_e^2)\Delta\phi''] \end{array} \right\} \quad (3d)$$

where $\Phi'' = \phi''_a + \phi''_b$. Owing to the hermiticity of the density matrix, $\rho^{(2)}_{gg'} = \rho^{(2)*}_{g'g}$ and $\rho_{ee'} = \rho^{(2)*}_{e'e}$.

After a time delay τ, the induced polarization $P^{(3)}(t)$ contains only matrix elements that oscillate with the transition frequency. Therefore, the emitted light carries spectroscopic information about the system. For equally chirped pulses, the intensity of each spectral line in the detection direction $\mathbf{k}_S = \mathbf{k}_a - \mathbf{k}_b + \mathbf{k}_c$, is given by the following expression:

$$I_{eg}(\tau) = I_g(\tau) + I_e(\tau) + I_c(\tau) \quad (4a)$$

with

$$I_g(\tau) \propto \left[1+\cos(\omega_e\tau_{ab})\cos\left(\frac{\phi''\omega_g\omega_e}{2}\right)\right] \times [\cos(\omega_g\tau)+1] \quad (4b)$$

$$I_e(\tau) \propto \left[1+\cos(\omega_g\tau_{ab})\cos\left(\frac{\phi''\omega_g\omega_e}{2}\right)\right] \times [\cos(\omega_e\tau)+1] \quad (4c)$$

and $I_c(\tau)$ is a contribution from less significant cross-terms that oscillate with linear combinations of both vibrational frequencies ω_g and ω_e. For unchirped pulses, setting $\tau_{ab} = (n+1/2)\tau_e$, where $\tau_e = 2\pi/\omega_e$, we obtain a signal that is characterized by the dynamics of the excited state and vice versa for $\tau_{ab} = (n+1/2)\tau_g$ with $\tau_g = 2\pi/\omega_g$.[16,17] Note that chirp only affects the vibrational coherence terms.[21] The control over the observed molecular dynamics is achieved using the vibrational time-scale of the system in each electronic state. The introduction of chirped pulses enhances or decreases the contribution of vibrational coherence terms to the signal such that the characterization of the molecular dynamics depends on both parameters. Because of the phase-matching detection at $\mathbf{k}_S = \mathbf{k}_a - \mathbf{k}_b + \mathbf{k}_c$ we ignore the signal that would be observed at $\mathbf{k}_S = -\mathbf{k}_a + \mathbf{k}_b + \mathbf{k}_c$, and also the non-coherent effects caused by the individual beams. The condition to have a signal that depends on ω_g is a non-zero population in several vibrational levels of the ground state initially. The expressions of Eqn (4) can be used to simulate the signal collected experimentally.[16,17]

EXPERIMENTAL

The experiments were carried out with 65 fs (FWHM when transform-limited) pulses centered at 620 nm generated by a CPM femtosecond laser system. After amplification by a four-stage dye amplifier pumped by a 30 Hz Nd : YAG laser, the pulses had an average pulse energy of 0.5 mJ. The beam was further attenuated to avoid saturation of transitions and high-intensity effects. This laser beam was split into three beams, each with energy per pulse of ~20 μJ, and combined at the sample by a 0.5 m focal length lens in the forward box geometry with 1 in sides.[22,23] The two diagonally opposed fields are labeled E_a and E_c and the field in the corner between them is labeled E_b. The time delay between the first two pulses (τ_{ab}) was controlled by a manual translator and the time delay between the second and third pulse (τ) was scanned in time by a computer-controlled actuator to yield the FWM signal transients. The pulses were focused into a quartz cell containing neat iodine vapor at 140 °C (optical density of the sample at 620 nm was <0.4 OD). The three-pulse FWM signal arising in the phase matching direction $\mathbf{k}_S = \mathbf{k}_a - \mathbf{k}_b + \mathbf{k}_c$ was spatially filtered and collected by a spectrometer for different wavelengths within the spectral range 605–635 nm. Unless noted otherwise, the spectral acceptance of the spectrometer was set to 2 nm. Each transient at a given wavelength was taken at 150 different time delays with 10 laser shots per point and averaged for 20 scans. The data were discriminated by the requirement that the energy of each laser pulse lies within one standard deviation from the mean. The transients collected at different wavelengths were combined into the contour diagrams where the darkest areas correspond to the highest values of the square root of the signal intensity. The two-dimensional data were obtained by interpolating the spectral profile using a multiple Gaussian fit to experimentally obtained spectrum.

To characterize the pulses and measure the chirp, a frequency-resolved optical gating (FROG) instrument was used. The pulses were chirped by the translation of the one of the prisms in the compression stage. The advantage of the three-pulse FWM method is that all the measurements presented here were taken with the same setup and conditions with the pulse sequence and pulse chirp as the only parameters that were changed. This point is of particular importance for the T_2 measurement on different electronic states.

RESULTS AND DISCUSSION

The polarization resulting from resonant three-pulse FWM experiments is typically long-lived[24] and therefore carries valuable spectroscopic information about the dynamics of the system. The intensity of the oscillations of the emitted light depends on the time delay τ. One can distinguish two components—one that oscillates with the vibrational frequency of the ground state and one that oscillates with the vibrational frequency of the excited state. Each contribution corresponds to the molecular dynamics in each electronic state and, by selecting the appropriate control parameters, one component can be enhanced with respect to the other.

In order to illustrate the importance of wavelength resolution in three-pulse FWM, we show data in Fig. 1 obtained for $\tau_{ab} = 0$ fs with transform-limited pulses. At the top of Fig. 1, the spectrally dispersed data show that the signal is a complex interplay between ground- and excited-state vibrational coherence with an underlying broad background that results most probably from off-resonance processes. The change of a spectroscopic feature as a function of the wavelength is due to a change of the vibrational population and coherence in each electronic state. The transient at the bottom of Fig. 1 was

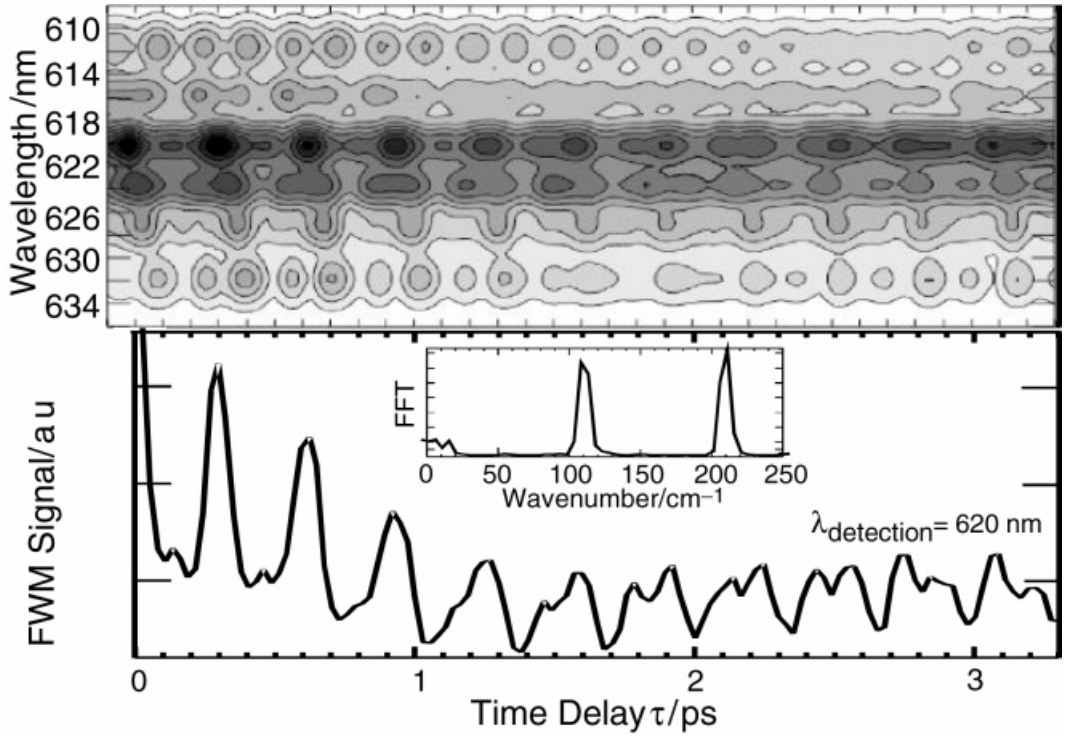

Figure 1. Spectrally dispersed time-resolved experimental data for three-pulse FWM with $\tau_{ab} = 0$ fs and transform-limited pulses. (Top) the first 3.3 ps of the data are presented as a contour plot where darker areas correspond to higher signal intensity. Both ground-(160 fs period) and excited-state (307 fs period) dynamics are observed with these experimental conditions. (Bottom) FWM data without spectral dispersion (broad bandwidth detection). The transient shows a mixture of ground- and excited-state dynamics that are evident in the Fourier transform (inset). It is clear that the two-dimensional contour contains more detailed information about the dynamics of the system.

obtained with broadband detection (8–16 nm). The power fast Fourier transform (FFT) of the data (inset) shows prominent peaks at 108 and 208 cm^{-1}, indicating excited- and ground-state vibrational coherence, respectively.

For this sequence, the first two pulses transfer population to both electronic states by four different FWM processes involving photon echo and virtual echo signals.[13,17] When the third pulse is applied, a non-linear polarization is induced on both populations and the spectroscopic information carried by the emitted light depends on the dynamics of both electronic states. The observation of ground- and excited-state dynamics in this type of measurement is consistent with observations from Keifer's group in a similar experiment on iodine using 573 nm excitation.[12]

In Fig. 2 we show spectrally dispersed data obtained as a function of τ when transform-limited pulses were applied for two different pulse sequences, (a) $\tau_{ab} = 614$ fs and (b) $\tau_{ab} = 460$ fs. The transients below the contour plots show a cut along a single wavelength ($\lambda = 619$ nm) to highlight the time-resolved dynamics arising from vibrational dynamics in the ground state (a) and the excited state (b). For $\tau_{ab} = 614$ fs, the signal oscillates with $\tau_g = 160$ fs corresponding to the molecular dynamics in the ground state for vibrational levels $v'' = 2–4$. There is a small contribution from the excited state that is apparent at 628 nm. The spectral data present a shift of about 80 fs between the FWM signal intensity maxima at 612 and 628 nm, primarily due to the anharmonicity of the excited state. The spectrally dispersed signal for $\tau_{ab} = 460$ fs [see Fig. 2(b)] can be assigned to the dynamics of the excited state with an oscillation period of $\tau_e = 307$ fs corresponding to vibrational levels $v' = 6–11$. No evidence of ground-state dynamics is evident in this transient.

From Fig. 2, it is clear that the pulse sequence allows us to isolate a desired electronic state to study its dynamics. To demonstrate the usefulness of this selectivity, we applied this technique to measure the vibrational coherence relaxation time of the ground and the excited states, $T_{2g'g}$ and $T_{2ee'}$ of iodine. In Fig. 3 we show the dephasing of the vibrational coherence (or T_2 process) for the (a) ground and (b) excited states. The corresponding transients are also shown for the first 15 ps, (c) and (d), respectively. From an exponential fit to the experimental data, we obtain $T_{2gg'} = 240 \pm 50$ ps and $T_{2ee'} = 210 \pm 50$ ps by multiplying the relaxation time by a factor of 2. The transient shown in Fig. 3(c) oscillates with a period $\tau_g = 160$ fs, characteristic of the ground state. Similarly, the transient shown in the Fig. 3(d) corresponds to the excited-state dynamics ($\tau_e = 307$ fs). These experiments were performed at 200 °C. The optical density at 620 nm was <0.4 OD. In both transients the rotational dynamics and vibrational revival are apparent. More detailed analysis of the relaxation experiment will be published elsewhere.[25]

Another example of the applicability of an FWM technique for the measurement of the collisional dephasing rate is the experiment on a gaseous system done by Prior's group. They measured the polarization dephasing time, T_2, of atomic potassium using an FWM setup with limited transfer, picosecond pulses, when the first two pulses overlap.[26,27] Our experimental data show that using the FWM technique with a specific pulse sequence, it is possible to measure selectively the relaxation time of a particular electronic state.

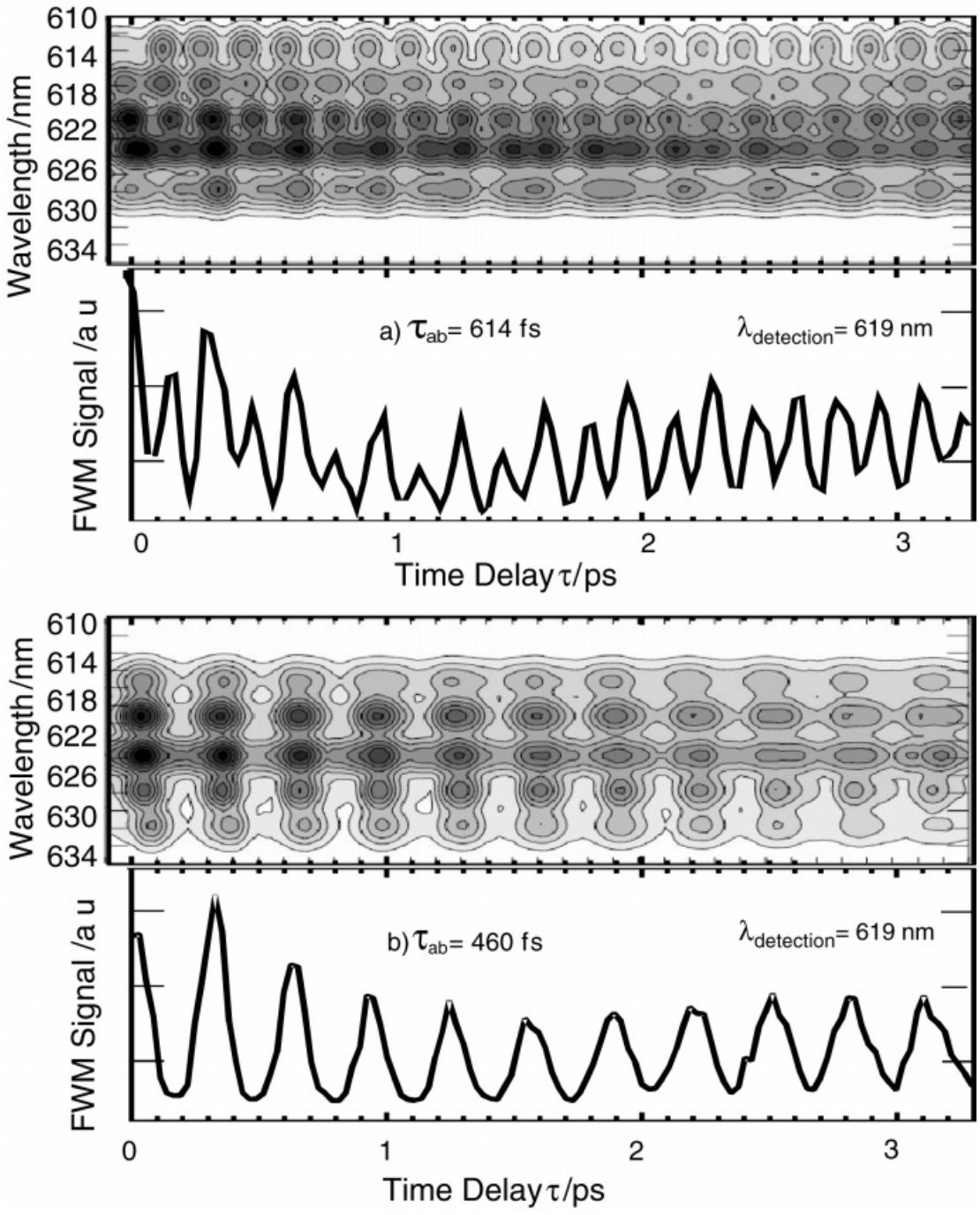

Figure 2. Spectrally dispersed time-resolved experimental data for three-pulse FWM. (a) FWM data obtained with $\tau_{ab} = 614$ fs and transform-limited pulses. The first 3.3 ps of the spectrally dispersed data are presented as a contour plot. The data show primarily ground-state vibrational coherence (160 fs period). A single transient detected with a narrow bandwidth at 619 nm is shown to illustrate these dynamics. The slight delay (~80 fs) between features at 611 and 627 nm is caused primarily by the anharmonicity of the excited state. (b) FWM data obtained with $\tau_{ab} = 460$ fs and transform-limited pulses. The first 3.3 ps of the spectrally dispersed data are presented as a contour plot. The data show primarily excited-state vibrational coherence (307 fs period). A single transient detected with a narrow bandwidth at 619 nm is shown to illustrate these dynamics and to demonstrate that ground-state coherence is not observed for this pulse sequence.

In order to explore the role of the pulse chirp in the control of the molecular dynamics, experimental data with $\tau_{ab} = 460$ fs was obtained when beams E_a and E_b are equally chirped, $\phi'' = +3300$ fs^2. The spectrally dispersed data for the above conditions are shown at the top of Fig. 4. From these data, it is clear that chirp pulses lead to an increased contribution from the ground state [see Fig. 2(b)]. Near the 620 nm region of the spectrum, the mixing of both states dynamics is evident, whereas for longer wavelength the excited state dynamics prevails. The data at the bottom of Fig. 4 are cuts at single detection wavelengths. Notice that a phase difference of ~150 fs occurs between the transient detected at 611 nm and that at 627 nm. These two transients show very little evidence of the ground-state vibrational dynamics. However, the transient obtained for detection at 618 nm seems to be dominated by contributions from ground-state vibrational dynamics. These complex dynamics could not be obtained

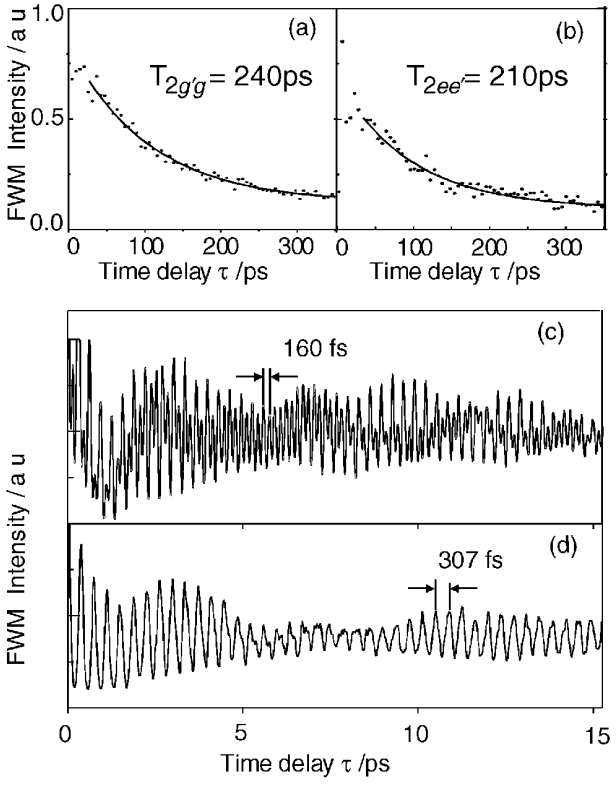

Figure 3. Measurements of vibrational coherence relaxation in the (a) ground and (b) excited states. The intensity of FWM emission is plotted as a function of time delay (τ) between pulses E_b and E_c. The time delay between pulses E_a and E_b is kept fixed at $\tau_{ab} = 614$ fs) for ground-state measurements and $\tau_{ab} = 460$ fs for excited-state measurements. The solid line is an exponential fit to the experimental data (dots). The first 15 ps of the measurements in (c) and (d) show the initial vibrational wave packet spreading and rotational dephasing. In each case, the vibrational period is indicated.

from spectrally integrated transients. For these measurements beam E_c was also chirped. The observed phase differences as a function of detection wavelength are consistent with the magnitude and sign of the laser chirp.

The theoretical analysis, performed on the basis of a four-level system, demonstrates that the control mechanism depends on the first two pulses. In previous work we have shown that the time delay between the second and third pulses can be used to isolate the excited-state dynamics.[16,17] However, the second time delay or the detection wavelength has no influence over the initial preparation. The molecular parameters of interest are the vibrational coherence and the population of each electronic state. The ground- and excited-state contributions observed in the signal are proportional to the respective vibrational coherence amplitudes.[21] Populations are not directly observed in our measurements but can be controlled using the appropriate pulse sequence and chirp, as discussed below.

The value that quantitatively describes the control of the population transfer is the spatially averaged amplitude of the grating formed by the molecules in the excited state:

$$\delta\rho = \left\langle \left| \sum_e \rho_{ee}^{(2)}(\tau_{ab}, \phi'') \right| \right\rangle_x \propto \{1 + \cos(\omega_e \tau_{ab}) \times \cos(\omega_g \tau_{ab}) + \cos[(\phi_b'' - \phi_a'')\omega_g \omega_e][\cos(\omega_e \tau_{ab}) + \cos(\omega_g \tau_{ab})]\}^{1/2} \quad (5)$$

After the interaction with the first pair of the pulses, a spatial grating appears in the sample formed by molecules in the excited state [Eqn (3)]. $\delta\rho$ is the amplitude of this transient grating when initially the molecules are equally distributed into the vibrational levels of the ground state. The expression in [Eqn (5)] applies to different experimental setups. When the first two pulses are collinear and phase-locked, maximum grating amplitudes can be achieved over the entire laser interaction region in the sample. The population of the excited state will depend in this case on the phase difference between the pulses, $\Delta\theta$ (not written explicitly),[28] and on the parameters ω_g, ω_e, τ_{ab} and ϕ'' as shown in Eqn (5). For non-collinear pulses a grating is always formed regardless of the optical phase difference of the pulses, and phase locking could be used to fix the spatial position of this grating. The amplitude of the grating for non-collinear cases is given by Eqn (5). The extent of the population transfer from the ground to the excited state is plotted in Fig. 5(a). When the first two pulses are equally chirped, $\phi_a'' = \phi_b''$, the chirp does not affect the population transfer [see Fig. 5(a)].[21,29]

In order to identify how vibrational coherence is manipulated by the use of pulse sequences and pulse chirps in the ground state, we define the coherence in the ground state as

$$C_g = \left\langle \left| \rho_{gg'}^{(2)}(\tau_{ab}, \phi'') \right| \right\rangle_x \propto \sqrt{1 + \cos(\omega_e \tau_{ab}) \cos\left[\tfrac{1}{2}(\phi_a'' + \phi_b'')\omega_g \omega_e\right]} \quad (6)$$

and the coherence in the excited state as

$$C_e = \left\langle \left| \rho_{ee'}^{(2)}(\tau_{ab}, \phi'') \right| \right\rangle_x \propto \sqrt{1 + \cos(\omega_g \tau_{ab}) \cos\left[\tfrac{1}{2}(\phi_a'' + \phi_b'')\omega_g \omega_e\right]} \quad (7)$$

These expressions allow us to evaluate the extent of vibrational coherence in the ground state and in the excited state as a function of chirp and time delay τ_{ab}. In these contour plots, we have only plotted positive chirp values. Because the simulations are symmetric with respect to the sign of the laser chirp, no anharmonic terms can be included in the four level model.

The amplitudes of excited and ground state vibrational coherence are plotted in Fig. 5(b) and 5(c). Note that in this case both τ_{ab} and chirp can be used interchangeably. The coherence of both electronic states will achieve their maximum value periodically for chirp values $\phi_c'' = 8\pi n/\omega_e \omega_g$. Close inspection of these plots indicates that the vibrational coherence is periodic with respect to τ_{ab}. A period of 160 fs is apparent from Fig. 5(b), corresponding to excited-state coherence, whereas a period of 307 fs, in Fig. 5(c), corresponds to the ground-state coherence. The vertical dashed lines in Fig. 5 correspond to the experimental values of $\tau_{ab} = 460$ and 614 fs. When the chirp is zero, the information obtained from Fig. 5 is supported by the experimental data in Fig. 2. Indeed, when $\tau_{ab} = 460$ fs only the excited-state coherence contributes to the signal [see Figs 2(a) and 5(b) and (c)], whereas for $\tau_{ab} = 614$ fs, the signal is mostly characterized by the ground-state dynamics [see Figs 2(b) and 5(b) and (c)]. The data in Fig. 5 shows a loss of selectivity brought about by the introduction of chirp. This change

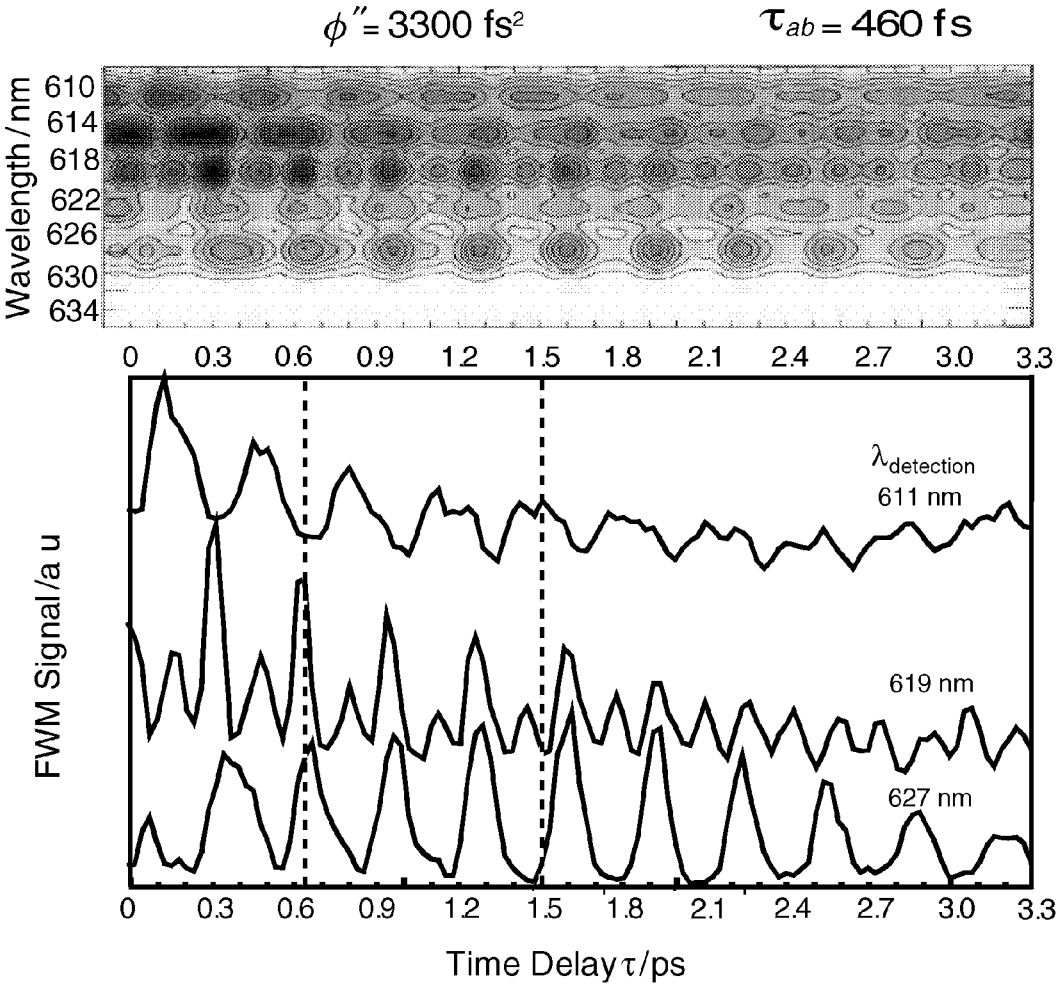

Figure 4. Spectrally dispersed time-resolved experimental data for three-pulse FWM. The FWM data were obtained with $\tau_{ab} = 460$ fs and $\phi'' = 3300$ fs^2. The first 3.3 ps of the spectrally dispersed data are presented as a contour plot. The data show a mixture of ground- and excited-state vibrational coherence. Single-wavelength detection transients detected with a narrow bandwidth are shown to illustrate some details about the observed dynamics. Vertical lines are used to indicate that the vibrational coherence detected at 611 nm is out-of-phase with the transient detected at 627 nm. This information would be lost in spectrally integrated FWM measurements.

can be followed in Fig. 5(c) and (b) going from chirp values of 0 to 3300 fs^2. In the case of chirped pulses with $\phi'' = 3300$ fs^2 and $\tau_{ab} = 460$ fs, the theory predicts a signal that mostly arises from the ground-state dynamics; this result is in excellent agreement with the experimental data shown in Fig. 4.

When the first two laser pulse chirp have equal magnitude but opposite sign ($\phi''_a = -\phi''_b$), the chirp magnitude can be used to control the population transfer [Fig. 6(a)]. Note that this transfer is at a maximum value for chirp values $\phi''_c = 4\pi n/\omega_e\omega_g$. Independent of the chirp [see Fig. 6(c)], the amplitude of the vibrational coherence in the ground state (C_g) achieves a maximum value when the time delay of a second pulse is equal to the vibrational period of the excited state. This time delay corresponds to the propagation time of the wave packet from time zero to the Franck–Condon region on the excited potential surface.

For chirped pulses with equal magnitude and sign, the vibrational coherence can be manipulated but the population transfer cannot. For oppositely chirped pulses, one can control the population transfer from the ground to the excited state, but the coherence transfer and hence the observed dynamics are not affected.

CONCLUSIONS

We have shown that the signal arising from time-resolved FWM measurements carries valuable information about the intramolecular dynamics of the system. The time delay between the first two pulses and the laser chirp are valuable parameters for controlling the population and coherence transfer. The theoretically calculated and experimentally observed effects indicate absolute control for the population and coherence transfer.

More specifically, we have explored the role of pulse sequence and pulse chirp. The characterization of the intramolecular dynamics was carried out by using spectrally dispersed FWM. We have shown that the two-dimensional data, detection wavelength and time delay, provide a wealth of spectroscopic information. Control over population and vibrational coherence has been demonstrated using specific pulse sequences. The ground-state dynamics, observed for $\tau_{ab} = 614$ fs, showed the signature of excited-state anharmonicity. The excited-state dynamics observed for $\tau_{ab} = 460$ fs were isolated. No ground-state dynamics were observed in this case for any of the detection wavelengths. Chirped pulses were used

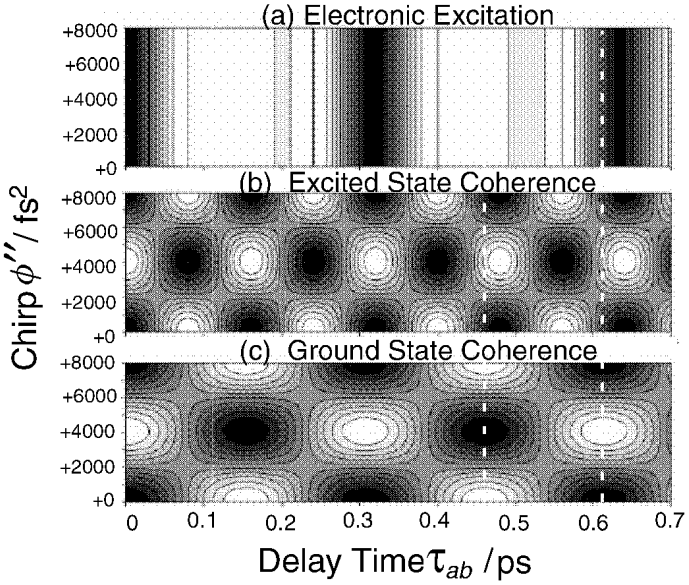

Figure 5. Simulations using Eqns (5)–(7) for the four-level system for equally chirped pulses (magnitude and sign). (a) This contour plot shows the amplitude of the excited-state population grating as a function of time delay and pulse chirp. This grating achieves a minimum for $\tau_{ab} = 153$ and 460 fs and a maximum for $\tau_{ab} = 0$, 307, and 614 fs. Note that the grating amplitude, which is related to the population transfer between the ground and excited electronic states, is not affected by the magnitude of the laser chirp. (b) Amplitude of the excited-state vibrational coherence. Note that the magnitude of excited-state coherence depends on the ground-state dynamics. This dependence is a result of the initial population of two vibrational ground-state levels. (c) Amplitude of the ground-state vibrational coherence. The amplitude depends on the excited-state dynamics and oscillates with a period of 307 fs. Note that for $\phi'' = 0$ fs^2, the ground-state coherence is at a minimum for $\tau_{ab} = 460$ fs and at a maximum for $\tau_{ab} = 614$ fs. This is consistent with the observed experimental data.

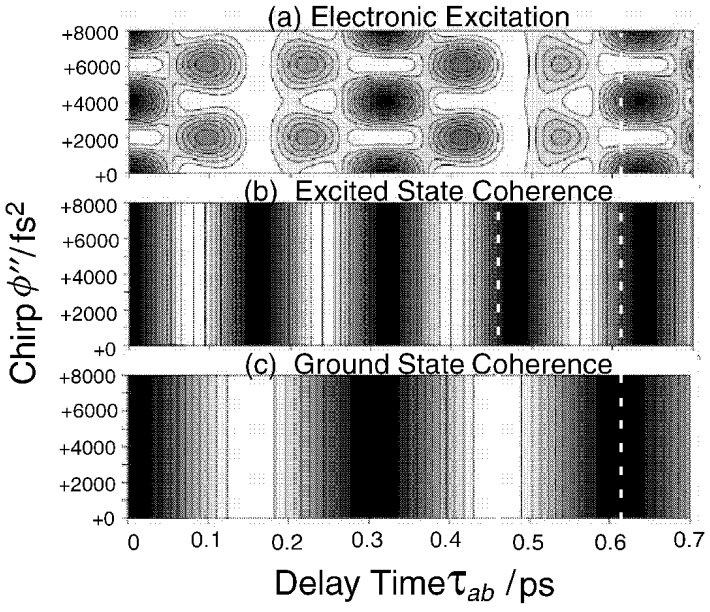

Figure 6. Simulations using Eqns (5)–(7) for the four-level system for chirped pulses with equal magnitude but opposite sign. (a) This contour plot shows the amplitude of the excited-state population grating as a function of time delay and pulse chirp. This grating achieves a minimum for $\tau_{ab} = 153$ and 460 fs and a maximum for $\tau_{ab} = 0$, 307, and 614 fs when the pulses are not chirped. Note that the grating amplitude, which is related to the population transfer between the ground and excited electronic states, depends on the magnitude of the pulse chirp. Amplitude of the (b) excited-state and (c) ground-state vibrational coherence. For this case the vibrational coherence is independent of the magnitude of the chirp.

to explore the process of vibrational coherence transfer. For these measurements, the spectrally resolved data showed that the vibrational features detected at shorter wavelengths lagged behind the features observed for longer wavelengths because of the positive chirp. This type of information would have been lost in a spectrally integrated measurement. The theoretical foundation for these observations based on a four-level density matrix formalism was found to be in remarkably good agreement with the observations. A prediction was made regarding chirped pulses with equal magnitude but opposite sign. For this case, the vibrational coherence transfer is not affected by the magnitude of the chirp but the population transfer is.

When the system contains a reactive pathway, coherence and population transfer can be used to enhance or

decrease the probability of the system for following that pathway. The coherence determines the dynamics of the system. In multidimensional systems, one may want to control the yield of different pathways or affect the rate of intramolecular vibrational relaxation.[30] This type of control, where the phase of the quantum-mechanical superpositions is manipulated by the optical phases of the pulses to determine the outcome of chemical reactions, results in true control of the final population transfer from reactant to product.[31–35] Alternatively, the first two pulses can be used to prepare the system in a specific superposition of states and a third pulse can be used to complete the chemical reaction.[36]

Based on these observations, we consider three-pulse FWM to be a powerful tool for learning about the intramolecular dynamics of molecular systems. Many of these ideas can be extended to larger molecules and into the condensed phase. With sufficiently short pulses, one is able to act with the first two pulses on a timescale that is faster than coherence relaxation. This statement can be supported by the observation of coherent vibrational dynamics in liquids.[37–39] We are considering extensions of this spectroscopic tool, providing two-dimensional information and selective excitation, to more complex systems.

Acknowledgements

This research was partially funded by a grant from the National Science Foundation (CHE-9812584). MD is a Lucille and David Packard Science and Engineering Fellow, a Camille Dreytus Teacher-Scholar, and an Alfred P. Sloan Fellow. EJB is supported by a National Science Foundation Graduate Fellowship. IP gratefully acknowledges a James L. Dye Endowment Fellowship.

REFERENCES

1. Heritage JP, Gustafson TK, Lin CH. *Phys. Rev. Lett.* 1975; **34**: 1299.
2. Lin CH, Heritage JP, Gustafson TK, Chiao RY, McTague JP. *Phys. Rev. A* 1976; **13**: 813.
3. Zewail AH (ed). *Femtochemistry*, vols I and II. World Scientific: Singapore, 1994.
4. Manz J, Woste L (eds). *Femtochemistry*, vols I and II. VHS: Heidelberg, 1995.
5. Chergui M (ed). *Femtochemistry: Ultrafast Chemical and Physical Processes in Molecular Systems*. World Scientific: Singapore, 1996.
6. Sundstrom V (ed). *Femtochemistry and Femtobiology*. World Scientific: Singapore, 1997.
7. Maas DJ, Duncan DI, Vrijen RB, van der Zande WJ, Noordam LD. *Chem. Phys. Lett.* 1998; **290**: 75.
8. Cao JS, Bardeen CJ, Wilson KR. *Phys. Rev. Lett.* 1998; **80**: 1406.
9. Scherer NF, Ruggiero AJ, Du M, Fleming GR. *J. Chem. Phys.* 1990; **93**: 856.
10. Schoenlein RW, Mittleman DM, Shiang JJ, Alivisatos AP, Shank CV. *Phys. Rev. Lett.* 1993; **70**: 1014.
11. Meshulach D, Silbergberg Y. *Nature (London)* 1998; **396**: 239.
12. Schmitt M, Knopp G, Materny A, Kiefer W. *Chem. Phys. Lett.* 1997; **280**: 339; Meyer S, Schmidt M, Materny A, Kiefer W, Engel V. *Chem. Phys. Lett.* 1999; **301**: 248.
13. Brown EJ, Zhang Q, Dantus M. *J. Chem. Phys.* 1999; **110**: 5772.
14. Schmitt M, Knopp G, Materny A, Kiefer W. *Chem. Phys. Lett.* 1997; **270**: 9.
15. Mukamel S. *Principles of Nonlinear Optical Spectroscopy*. Oxford University Press: New York, 1995.
16. Brown EJ, Pastirk I, Grimberg BI, Lozovoy VV, Dantus M. *J. Chem. Phys.* 1999; **111**: 3779.
17. Pastirk I, Brown EJ, Grimberg BI, Lozovoy VV, Dantus M. *Faraday Discuss. Chem. Soc.* 1999; **113**: 401.
18. Bloembergen N, Lotem H, Lynch RT. *Indian J. Pure Appl. Phys.* 1978; **16**: 151.
19. Allen L, Eberly JH. *Optical Resonance and Two-Level Atoms*. Wiley: New York, 1975.
20. Boyd RW. *Nonlinear Optics*. Academic Press: San Diego, 1992.
21. Pastirk I, Lozovoy VV, Grimberg BI, Brown EJ, Dantus M. *J. Phys. Chem. A* 1999; **103**: 10226.
22. Prior Y. *Appl. Opt.* 1980; **19**: 1741.
23. Shirley JA, Hall RJ, Eckbreth AC. *Opt. Lett.* 1980; **5**: 380.
24. Weiner AM, Silvestri SD, Ippen EP. *J. Opt. Soc. Am. B* 1985; **2**: 654.
25. Lozovoy VV, Pastirk I, Dantus M. *J. Chem. Phys.* in review.
26. Kinrot O, Prior Y. *Phys. Rev. A* 1994; **50**: 1999.
27. Kinrot O, Prior Y. *Phys. Rev. A* 1995; **51**: 4996.
28. Pshenichnikov MS, Boeij WPd, Wiersma DA. *Phys. Rev. Lett.* 1996; **76**: 4701.
29. Shen YC, Cina JA. *J. Chem. Phys.* 1999; **110**: 9793.
30. Pastirk I, Brown EJ, Zhang Q, Dantus M. *J. Chem. Phys.* 1998; **108**: 4375.
31. Melinger JS, Hariharan A, Gandhi SR, Warren WS. *J. Chem. Phys.* 1991; **95**: 2210.
32. Broers B, van Linden van den Heuvell HB, Noordam LD. *Phys. Rev. Lett.* 1992; **69**: 2062.
33. Bardeen CJ, Che J, Wilson KR, Yakovlev VV, Cong P, Kohler B, Krause JL, Messina M. *J. Phys. Chem. A* 1997; **101**: 3815.
34. Bardeen CJ, Yakovlev V, Squier JA, Wilson KR. *J. Am Chem. Soc.* 1998; **120**: 13023.
35. Yakovlev V, Bardeen CJ, Che J, Cao J, Wilson KR. *J. Chem. Phys.* 1998; **108**: 2309.
36. Pausch R, Heid M, Chen T, Kiefer W, Schwoerer H. *J. Chem. Phys.* 1999; **110**: 9560.
37. Ruhman S, Joly AG, Nelson KA. *J. Chem. Phys.* 1987; **86**: 6563.
38. Banin U, Waldman A, Ruhman S. *J. Chem. Phys.* 1992; **96**: 2416.
39. Pugliano N, Palit DK, Szarka AZ, Hochstrasser RM. *J. Chem. Phys.* 1993; **99**: 7273.

